The Brownian Oscillator Model for Solvation Effects in Spontaneous Light Emission and Their Relationship to Electron Transfer

Bulang Li,† Alan E. Johnson, Shaul Mukamel,‡ and Anne B. Myers*,‡

Contribution from the Department of Chemistry and Center for Photoinduced Charge Transfer, University of Rochester, Rochester, New York 14627-0216

Received March 23, 1994®

Abstract: The Brownian oscillator model for the coupling of solvent motions to a solute's electronic transitions is applied to the calculation of absorption, relaxed fluorescence, and unrelaxed total emission (Raman and fluorescence) band shapes of a diatomic molecule in solution. The band shapes and the ratios of sharp scattering to broad fluorescence are explored as a function of the laser detuning from resonance, the parameters describing the solvent oscillator, and the excited-state lifetime, and direct comparisons with the stochastic theory, which does not contain the solvent-induced Stokes shift, are made. The relationship between the optical band shapes and the nuclear Franck−Condon factor for nonphotochemical electron transfer processes is also discussed within the Brownian oscillator model for the solvation coordinate. The limits of applicability of the "high-temperature" limit for the Brownian oscillator are established.

Introduction

Solvent−solute interactions in the liquid state play a major role in determining the line shapes and intensities of spectroscopic transitions, energy relaxation and dephasing processes, and chemical reaction rates through both static and dynamic effects. Due to the disordered but rapidly fluctional nature of the liquid state, the instantaneously different local environments experienced by different solute molecules in a dilute solution interconvert rapidly on the time scale of many experimental measurements. However, a variety of spectroscopic, physical, and chemical processes of interest do occur on time scales that are comparable to those for solvent motion, and there has been considerable recent activity in experimental and theoretical probes of the relationship between solvent dynamics and such processes as spontaneous light emission, pump-probe spectroscopies, electronic and vibrational dephasing, activated and barrierless chemical reaction rates, and electron transfer reactions.

Quantum mechanical coherences play an important role in most spectroscopic and some fast kinetic processes. Since it is usually not practical to treat all of the solvent degrees of freedom explicitly, a density matrix approach is generally used to allow averaging over the "uninteresting" bath degrees of freedom while treating the solute in a more detailed fashion. For condensed phase problems the coupling of the solute's energy levels to the environment has most often been treated through the stochastic model originally due to Bloembergen, Purcell, and Pound,[1] Anderson,[2] and Kubo.[3,4] This model assumes a Gaussian−Markovian process for the correlation function of the solvent-induced shifts of the solute energy levels and allows continuous interpolation between the "homogeneous" (fast modulation, motionally narrowed) and "inhomogeneous" (static) broadening limits. Such treatments successfully describe both resonance Raman scattering, a coherent two-photon process determined by the off-diagonal elements of the density matrix, and fluorescence, an incoherent component determined by the diagonal elements of the density matrix.[5−11] The partitioning of the total emission spectrum between resonance Raman scattering and fluorescence has been shown, both theoretically and experimentally, to be strongly dependent on the electronic dephasing caused by solvent modulation of the electronic transitions under consideration.[9,12,13] The solvent-induced broadening in optical spectroscopy can thus serve as a direct probe of both the strength and the time scale of the solvent−solute interactions.

Electron transfer reactions in liquids also depend on both static and dynamic aspects of the solvent−solute interactions. Electron transfer rates are usually described in terms of Golden Rule expressions which are valid in the nonadiabatic limit where the electronic coupling between the donor and the acceptor is weak.[14] The corresponding expressions for the charge-transfer absorption and emission band shapes treat the low-frequency solvent modes classically and incorporate their contribution to the optical processes through the solvent reorganization energy λ_S.[15] The Gaussian dependence of both the electron transfer rate and the optical absorption and emission line shapes as a

* Author to whom correspondence should be addressed.
† Present address: Department of Chemistry, University of California, La Jolla, CA 92093.
‡ Center for Photoinduced Charge Transfer.
® Abstract published in *Advance ACS Abstracts,* November 1, 1994.

(1) Bloembergen, N.; Purcell, E. M.; Pound, R. V. *Phys. Rev.* **1948**, *73*, 679.
(2) Anderson, P. W.; Weiss, P. R. *Rev. Mod. Phys.* **1953**, *25*, 269.
(3) Kubo, R. In *Fluctuation, relaxation, and resonance in magnetic systems*; ter Haar, D., Ed.; Oliver and Boyd: Edinburgh, 1962; p 23.
(4) Kubo, R. *Pure Appl. Chem.* **1985**, *57*, 201.
(5) Takagahara, T.; Hanamura, E.; Kubo, R. *J. Phys. Soc. Jpn.* **1977**, *43*, 802.
(6) Mukamel, S. *J. Chem. Phys.* **1985**, *82*, 5398.
(7) Lee, D.; Albrecht, A. C. *Adv. Infrared Raman Spectrosc.* **1985**, *12*, 179.
(8) Sue, J.; Yan, Y. J.; Mukamel, S. *J. Chem. Phys.* **1986**, *85*, 462.
(9) Yan, Y. J.; Mukamel, S. *J. Chem. Phys.* **1987**, *86*, 6085.
(10) Watanabe, J.; Kinoshita, S.; Kushida, T. *J. Chem. Phys.* **1987**, *87*, 4471.
(11) Nibbering, E. T. J.; Duppen, K.; Wiersma, D. A. *J. Chem. Phys.* **1990**, *93*, 5477.
(12) Hochstrasser, R. M.; Nyi, C. A. *J. Chem. Phys.* **1979**, *70*, 1112.
(13) Myers, A. B.; Li, B. *J. Chem. Phys.* **1990**, *92*, 3310.
(14) Jortner, J.; Bixon, M. *J. Chem. Phys.* **1988**, *88*, 167.
(15) Marcus, R. A. *J. Phys. Chem.* **1989**, *93*, 3078.

0002-7863/94/1516-11039$04.50/0

function of the standard free energy change for the reaction, $\Delta G°$, emphasizes the fact that both the optical and the rate processes are governed by the same solvent−solute interaction parameters,[15,16] and the existence of the Marcus inverted region becomes more physically intuitive when the connection between the electron transfer and optical processes is made (i.e. the inverted region corresponds to the high-frequency side of the optical absorption spectrum). Furthermore, Mukamel and co-workers derived expressions for the electron transfer rate in condensed phase from the same material response functions used to describe linear and nonlinear spectroscopies, establishing the intimate relationship between charge transfer and optical spectroscopy even in the strong coupling (adiabatic) limit.[17,18] Yet in spite of the similarities between charge-transfer optical spectroscopies and electron transfer rates, the models used to treat the solvation coordinate for these two processes are generally very different. The standard treatments of both charge-transfer absorption band shapes and nonadiabatic electron transfer reactions implicitly assume, by using a Gaussian line shape, that the solvent-induced spectral broadening is in the static, inhomogeneous limit. At the same time, many analyses of emission yields and band shapes in other molecular systems based on stochastic models indicate that the static limit is not appropriate,[8,13,19−22] and a recent resonance Raman study of an organic charge-transfer complex also found that a significant amount of "homogeneous" solvent-induced broadening was needed to explain the absolute Raman intensities.[23] While the solvent-induced broadening need not be slow on the Raman time scale to generate a nearly Gaussian contribution to the line shape,[8,9,13] these results do suggest that the assumption of a static Gaussian solvent contribution to both optical charge-transfer spectra and electron transfer rate versus driving force curves may need to be reevaluated.

A principal source of the dichotomy between the models used to describe solvent−solute interactions in the spectroscopic and charge-transfer applications is that the stochastic model commonly employed in spectroscopic applications misses one of the aspects of solvation that is central to charge-transfer processes: the solvent Stokes shift. This is because the stochastic model describes only the effect of the solvent on the solute, but not vice versa; i.e., the effect of the change in the solute's electronic state on the solvent, which is responsible for the Stokes shift of absorption relative to fluorescence, is not included. This effect is clearly important in optical or rate processes that involve large shifts in electron density and are carried out in polar solvents. In this study we employ a more complete model for the solvent−solute interaction, the Brownian oscillator, to illustrate the solvent effects on optical absorption and emission line shapes and their relation to electron transfer processes. Damped oscillator models for the solvation coordinate have been employed in describing both optical absorption and emission line shapes and various nonlinear optical processes.[22,24−30] Here we apply this model to the calculation of unrelaxed (Raman and fluorescence) spectra. The simplified expressions often used to describe optical and rate processes in charge transfer systems, and the stochastic model often used to describe linear and nonlinear spectroscopies, can be shown to be special cases of the Brownian oscillator model in the static and high-temperature limits, respectively.

Theory

To describe the line shapes of optical absorption and emission spectra and electron transfer rates in condensed phases, we consider two solute electronic states, $|a\rangle$ and $|b\rangle$, coupled to a solvent degree of freedom. In spectroscopy $|a\rangle$ and $|b\rangle$ refer to the ground and excited electronic states, respectively, while for electron transfer they refer to the reactant and product states, respectively. In both processes the total Hamiltonian of the system can be written as

$$H_T = H + H_{int} \tag{1}$$

where the molecular Hamiltonian is

$$H = |g\rangle H_g \langle g| + |e\rangle H_e \langle e| \tag{2}$$

H_g and H_e, which both contain a solvent contribution, are the Hamiltonians for nuclear motion of the system when the solute is in electronic states $|g\rangle$ and $|e\rangle$, respectively. In the optical process H_{int} describes the interaction between the system and the electromagnetic field:

$$H_{int,opt} = -\mu E(\mathbf{r},t)(|g\rangle\langle e| + |e\rangle\langle g|) \tag{3}$$

where μ is the transition dipole of the system and $E(\mathbf{r},t)$ is the radiation field which is treated either classically or quantum mechanically depending on the optical process under consideration. For electron transfer, H_{int} accounts for the electronic coupling between the reactant and product states:

$$H_{int,et} = V(|g\rangle\langle e| + |e\rangle\langle g|) \tag{4}$$

where V is the coupling strength between $|g\rangle$ and $|e\rangle$.

A single classical field interacting with the two-level system described above induces a first-order polarization due to the linear optical response of the medium, resulting in the following line shape for optical absorption:[26,31]

$$I(\omega_L) = -2 \text{ Im } [J(\omega_L)] \tag{5}$$

where "Im" denotes the imaginary part, and $J(\omega)$, which has contributions from both the molecular Hamiltonian and the solvent motions, is the linear response function resulting from evolving the density matrix to first order in the radiation−matter interaction. This linear response function also gives the nuclear contribution to the electron transfer rate in the weak coupling (nonadiabatic) limit,[17,18] as discussed further below.

(16) Gould, I. R.; Noukakis, D.; Gomez-Jahn, L.; Young, R. H.; Goodman, J. L.; Farid, S. *Chem. Phys.* **1993**, *176*, 439.
(17) Yan, Y. J.; Sparpaglione, M.; Mukamel, S. *J. Phys. Chem.* **1988**, *92*, 4842.
(18) Yan, Y. J.; Mukamel, S. *J. Phys. Chem.* **1989**, *93*, 6991.
(19) Yang, T.-S.; Myers, A. B. *J. Chem. Phys.* **1991**, *95*, 6207.
(20) Myers, A. B.; Mathies, R. A. In *Biological Applications of Raman Spectroscopy*; Spiro, T. G., Ed.; Wiley: New York, 1987; Vol. 2, p 1.
(21) Sue, J.; Mukamel, S.; Okamoto, H.; Hamaguchi, H.; Tasumi, M. *Chem. Phys. Lett.* **1987**, *134*, 87.
(22) Nibbering, E. T. J.; Duppen, K.; Wiersma, D. A. *J. Photochem. Photobiol. A* **1992**, *62*, 347.
(23) Markel, F.; Ferris, N. S.; Gould, I. R.; Myers, A. B. *J. Am. Chem. Soc.* **1992**, *114*, 6208.
(24) Gu, Y.; Widom, A.; Champion, P. M. *J. Chem. Phys.* **1994**, *100*, 2547.
(25) Bosma, W. B.; Yan, Y. J.; Mukamel, S. *Phys. Rev. A* **1990**, *42*, 6920.
(26) Mukamel, S.; Yan, Y. J. In *Recent trends in Raman spectroscopy*; Banerjee, S. B., Jha, S. S., Eds.; World Scientific: Singapore, 1989; p 160.
(27) Nibbering, E. T. J.; Wiersma, D. A.; Duppen, K. *Chem. Phys.* **1994**, *183*, 167.
(28) Cong, P.; Deuel, H.; Simon, J. D.; Yan, Y. J. In *Ultrafast Processes in Chemistry and Photobiology*; El-Sayed, M. A., Molin, Y. N., Tanaka, I., Eds.; Blackwell Publishers: Brookline Village, in press.
(29) Cho, M.; Fleming, G. R. *J. Phys. Chem.* **1994**, *98*, 3478.
(30) de Boeij, W. P.; Pshenichnikov, M. S.; Duppen, K.; Wiersma, D. A. *Chem. Phys. Lett.* **1994**, *224*, 243.
(31) Mukamel, S. *Principles of nonlinear optical spectroscopy*; Oxford University Press: New York, in press.

Using the quantum description of the radiation field and calculating the perturbed density matrix to third order, the emission line shape is obtained as:

$$I(\omega_L,\omega_S) = 2\,\mathrm{Im}\,[R_1(\omega_s,0,\omega_L) + R_2(\omega_S,0,-\omega_L) + R_3(\omega_S,\omega_S-\omega_L,-\omega_L)] \quad (6)$$

where ω_L and ω_S are the incident and emitted frequencies, and R_1, R_2, and R_3, which also contain contributions from both solvent and solute, are the third-order nonlinear response functions.[26,31] The rate of electron transfer for arbitrary coupling strengths can also be evaluated using Liouville space projection operators at the same level of density matrix propagation.[17,18] Thus, upon the establishment of a model for the solvent−solute interaction, both the line shapes of the optical processes and the rate of electron transfer can be rigorously calculated using the above eqs 5 and 6, and eq II-24 in ref 17.

We consider here a molecular system containing a solute with a single harmonic mode coupled to a solvent degree of freedom which is described as a single-mode Brownian oscillator.[25,31] The Hamiltonians H_g and H_e are given by

$$H_g = (1/2)\hbar\omega(p^2 + q^2) + H_B(q_{B,g}) \quad (7)$$

and

$$H_e = (1/2)\hbar\omega[p^2 + (q + D)^2] + E_0 + H_B(q_{B,e}) \quad (8)$$

where ω is the frequency of the molecular mode, p and q are its dimensionless momentum and coordinate, and D is a dimensionless displacement of the equilibrium position between the two electronic states. (To avoid having the symbol Δ refer to two different physical quantities, in this paper we use D for the excited-state displacement along a vibrational mode, while Δ is the magnitude of the line broadening as discussed below. This notation is consistent with that used in refs 8, 9, and 26, for example, but reversed from that of ref 23.) H_B is the solvent mode Hamiltonian described by a frequency ω_B, displacement D_B, and coordinate q_B, where $q_{B,e} = q_{B,g} + D_B$, which obeys the Langevin equation:

$$\ddot{q}_B + \gamma\dot{q}_B + \omega_B{}^2 q_B = f(t) \quad (9)$$

where $f(t)$ is a random Langevin force and γ is the friction.

The shift and broadening of the electronic transition due to nuclear motions can be described by a total reorganization energy, $\hbar\lambda$, and a magnitude of broadening, Δ, which have contributions from both the high-frequency molecular mode (undamped harmonic oscillator) and the low-frequency solvent mode (Brownian oscillator). The following relations hold in general:

$$\lambda = \lambda_v + \lambda_S \quad (10)$$

with $\lambda_v = \omega D^2/2$ and $\lambda_S = \omega_B D_B{}^2/2$, and

$$\Delta^2 = \Delta_v{}^2 + \Delta_S{}^2 \quad (11)$$

with $\Delta_v{}^2 = \lambda_v\omega(2\bar{n}_v + 1)$ and $\Delta_S{}^2 = \lambda_S\omega_B(2\bar{n}_B + 1)$, where $\bar{n}_v$ and $\bar{n}_B$ are the thermally averaged occupation numbers of the molecular mode and the solvent mode, respectively. These quantities are given by[17]

$$\bar{n}_v = [\exp(\hbar\omega/k_BT) - 1]^{-1} \quad (12)$$

and

$$\bar{n}_B = [\exp(\hbar\omega_B/k_BT) - 1]^{-1} \quad (13)$$

where k_B is Boltzmann's constant. In spectroscopy, λ_v is the red shift of the emission (or blue shift of the absorption) due to the displacement between the ground and the excited electronic state surface along the solute vibrational coordinate; λ_S is the solvent contribution to this shift. In electron transfer, $\hbar\lambda_v$ and $\hbar\lambda_S$ represent the intramolecular and solvent reorganization energies, respectively.

For the molecular mode, we assume $\hbar\omega \gg k_BT$, so $\bar{n}_v = 0$ and $\Delta_v{}^2 = \lambda_v\omega$. For the solvent mode, we assume $\hbar\omega_B \ll k_BT$ (high-temperature limit; see Discussion) which leads to $\Delta_S{}^2 = 2\lambda_S k_BT/\hbar$.

The optical absorption line shape is given by

$$I(\omega_L) = -2\,\mathrm{Im}\sum_{a,b} P(a)|\mu_{ab}|^2 J_0(\omega_L - \omega_{ba} + i\gamma_{ba}) \quad (14)$$

while the fluorescence line shape for the case of complete vibrational relaxation prior to emission is

$$I(\omega_S) = 2\,\mathrm{Im}\sum_{a,b} P(b)|\mu_{ab}|^2 J_0{}^*(\omega_{ba} - \omega_S + i\gamma_{ba}) \quad (15)$$

Here a and b denote the vibrational levels of the ground and excited electronic state, respectively, $P(a)$ and $P(b)$ are the thermal equilibrium vibronic populations of levels a and b, γ_{ba} is the lifetime-limited width of the a ↔ b transition, and μ_{ab} is the electronic transition moment between states $|a\rangle$ and $|b\rangle$, which can generally be divided into a purely electronic factor and a nuclear Franck−Condon factor under the Born−Oppenheimer approximation. $J_0(\omega)$ here represents a purely solvent contribution to the line shape which can be calculated from[26,31]

$$J_0(\omega) = -i\int_0^\infty d\tau\,\exp(i\omega\tau)\,J_0(\tau) \quad (16)$$

and

$$J_0(\tau) = \exp[-g(\tau)] \quad (17)$$

For the Brownian oscillator model in the high-temperature and high-friction Smulochowski limits ($\Delta_S{}^2 = 2\lambda_S k_BT/\hbar$ and $\gamma \gg 2\omega_B$), the line shape function $g(\tau)$ is given by[25]

$$g(\tau) = (\Delta_S/\Lambda)^2[\Lambda\tau - 1 + \exp(-\Lambda\tau)] + i(\lambda_S/\Lambda)[1 - \exp(-\Lambda\tau)] \quad (18)$$

where Λ is the modulation frequency of the solvent oscillator, given by $\tau_L{}^{-1}$ where τ_L is the longitudinal relaxation time of a Debye solvent. If we neglect the imaginary term in the above equation (which can be shown to be equivalent to assuming infinite temperature),[31] the stochastic model for optical line broadening is obtained. The resulting purely real damping function broadens the absorption and emission spectra but cannot account for the solvent-induced Stokes shift of the emission spectrum.

Evaluation of the third-order nonlinear response functions using the Brownian oscillator model results in the following expression for the total emission (Raman and fluorescence) line shape when vibrational relaxation is neglected:

$$I(\omega_L,\omega_S) = 2\,\mathrm{Im}\sum_{a,b,c,d} P(a)\mu_{ab}\mu_{bc}\mu_{cd}\mu_{da}\sum_{n=0}^{\infty}\times$$

$$\left[\frac{(-1)^n z^n}{n!}\frac{J_n^*(\omega_{dc}-\omega_S+i\gamma_{dc})\tilde{J}_n(\omega_L-\omega_{da}+i\gamma_{da})}{\omega_{db}-i(\gamma_{db}+n\Lambda)}+\right.$$

$$\frac{(z^*)^n}{n!}\frac{J_n^*(\omega_{dc}-\omega_S+i\gamma_{dc})\tilde{J}_n^*(\omega_L-\omega_{ba}+i\gamma_{ba})}{\omega_{bd}+i(\gamma_{db}+n\Lambda)}+$$

$$\left.\frac{(z^*)^n}{n!}\frac{J_n(\omega_S-\omega_{dc}+i\gamma_{dc})J_n^*(\omega_L-\omega_{ba}+i\gamma_{ba})}{\omega_L-\omega_S-\omega_{ca}-i(\gamma_{ac}+n\Lambda)}\right] \quad (19)$$

where {a,c} denote the vibronic levels in the ground electronic state and {b,d} are those in the excited state, ω_{ij} is the frequency difference between levels i and j, and γ_{ij} is the homogeneous line width of the i to j transition. The nonlinear response functions of the solvent in eq (19) can be calculated from[17,26]

$$J_n(\omega) = i\int_0^\infty dt\,\exp(i\omega t)\,\exp[-g(t)][1-\exp(-\Lambda t)]^n \quad (20)$$

and

$$\tilde{J}_n(\omega) = i\int_0^\infty dt\,\exp(i\omega t)\,\exp[-g(t)]\left[\frac{z^*}{z}-\exp(-\Lambda t)\right]^n \quad (21)$$

where $z = (\Delta_S/\Lambda)^2 - i\lambda_S/\Lambda$.

If the time scale for vibrational relaxation is comparable to or shorter than the excited-state lifetime, it must be incorporated in evaluating the density matrix which then evolves through six instead of three independent pathways in Liouville space. Equation 19 can be modified to account for vibrational relaxation by introducing a phenomenological damping matrix as discussed in ref 32. We do not explore the effects of vibrational relaxation in the present work.

The standard Golden Rule expression for a radiationless transition (e.g. nonphotochemical electron transfer)[14,33,34] between vibrational levels of two different electronic manifolds can also be written in a form analogous to that of eqs 14 and 15:

$$k = \frac{2\pi}{\hbar}|V|^2\,\mathrm{Im}\frac{1}{\pi\hbar}\sum_{a,b}P(b)|\langle b|a\rangle|^2 J_0^*(\omega_{ba}+i\gamma_{ba}) \quad (22)$$

This expression is expected to hold for electron transfer deep in the Marcus inverted region, where activated barrier crossing makes a negligible contribution to the rate. Here V is the electronic matrix element which is taken to be independent of vibrational coordinate, while $|\langle b|a\rangle|^2$ is a vibrational Franck–Condon factor. This expression is essentially identical to eq 15 for fluorescence,[15,16,35] with the photon frequency set to zero and the matrix element μ_{ab} replaced by $V\langle b|a\rangle$. A general formula for the rate of electron transfer, valid across the range of coupling strengths from nonadiabatic to fully adiabatic, can also be developed as described in refs 17 and 36 from the above nonlinear response functions (eqs 20 and 21) with the Brownian oscillator model for the solvent–solute interaction.

The connection between the expressions given thus far and traditional electron transfer theory can be seen easily by letting the solvent dynamics approach the static limit ($\tau_L \to \infty$). In this case, $g(\tau)$ becomes $\Delta_S^2\tau^2/2 + i\lambda_S\tau$, and if we further neglect the lifetime broadening γ_{ba} relative to the solvent-induced breadth, eq 22 for the electron transfer rate becomes

$$k = \frac{2\pi}{\hbar}|V|^2\sum_{a,b}P(b)|\langle b|a\rangle|^2(4\pi\hbar\lambda_S k_B T)^{-1/2}\times \exp\left[\frac{-(\Delta G_{ba}^\circ/\hbar+\lambda_S)^2}{4\lambda_S k_B T/\hbar}\right] \quad (23)$$

where we define $\Delta G_{ba}^\circ = \hbar\omega_{ab}$. This gives the familiar parabolic dependence of ln k on driving force. In the same notation, eqs 14 and 15 for the optical absorption and emission spectra in the static limit become the expressions given by Marcus:[15]

$$I(\omega_L) \propto \sum_{a,b}P(a)|\mu_{ab}|^2(4\pi\lambda_S k_B T)^{-1/2}\times \exp\left[\frac{-(\Delta G_{ab}^\circ/\hbar+\lambda_S-\omega_L)^2}{4\lambda_S k_B T/\hbar}\right] \quad (24)$$

and

$$I(\omega_S) \propto \sum_{a,b}P(b)|\mu_{ab}|^2(4\pi\lambda_S k_B T)^{-1/2}\times \exp\left[\frac{-(\Delta G_{ba}^\circ/\hbar+\lambda_S+\omega_S)^2}{4\lambda_S k_B T/\hbar}\right] \quad (25)$$

where ΔG_{ab}° and ΔG_{ba}° are the driving forces for the forward (a to b) and backward (b to a) processes, respectively.

Results

We calculate all absorption line shapes from eq 14, relaxed emission from eq 15, and unrelaxed emission from eq 19. Note that overall multiplicative factors of ω_L for absorption and $\omega_L\omega_S^3$ for emission have been suppressed in these expressions. All calculations assume $k_BT = 200$ cm^{-1} ($T = 15$ °C). In all but Figure 6, we use homogeneous line widths of $\gamma_{ac}/2\pi c = 4$ cm^{-1} and $\gamma_{bd}/2\pi c = 10$ cm^{-1} for all pairs of ground (a,c) and excited state (b,d) vibrational levels; 10 cm^{-1} is also used for the vibronic line widths, e.g. $\gamma_{ba}/2\pi c$. We assume a single-mode (i.e. diatomic) solute having a vibrational frequency of 1500 cm^{-1} and a dimensionless displacement of $D = 0.9$, and model the solvent as a single-mode Brownian oscillator. Except for Figure 2, all calculations assume slow modulation, $\kappa = \Lambda/\Delta_S = 0.1$, which makes the solvent contribution to the line shape nearly Gaussian.

Figure 1 compares the absorption and unrelaxed emission line shapes in such a system with those calculated using the stochastic model for the solvent. Different zero–zero frequencies have been chosen for the two models so that they give the same calculated absorption maxima. The solvent parameters of $\Delta_S/2\pi c = 432$ cm^{-1} and $\Lambda/2\pi c = 43.2$ cm^{-1} correspond to a solvent reorganization energy of $\lambda_S/2\pi c = 467$ cm^{-1} (high-temperature limit) and a relaxation time of $\tau_L = \Lambda^{-1} = 123$ fs. The emission line shapes calculated from both solvent models contain a broad fluorescence band as well as sharp features due to Rayleigh and Raman scattering. The sharp scattering bands have line widths of 4 cm^{-1} due to vibrational dephasing in the ground electronic state, while the fluorescence and absorption band widths of 500 cm^{-1} (half-width at half-maximum) for each vibronic level are dominated by the solvent-induced electronic pure dephasing. In the Brownian oscillator model the absorption

(32) Sue, J.; Mukamel, S. *J. Opt. Soc. Am. B* **1988**, *5*, 1462.
(33) Marcus, R. A. *J. Chem. Phys.* **1984**, *81*, 4494.
(34) Ulstrup, J.; Jortner, J. *J. Chem. Phys.* **1975**, *63*, 4358.
(35) Myers, A. B. *Chem. Phys.* **1994**, *180*, 215.
(36) Mukamel, S.; Yan, Y. J. *Acc. Chem. Res.* **1989**, *22*, 301.

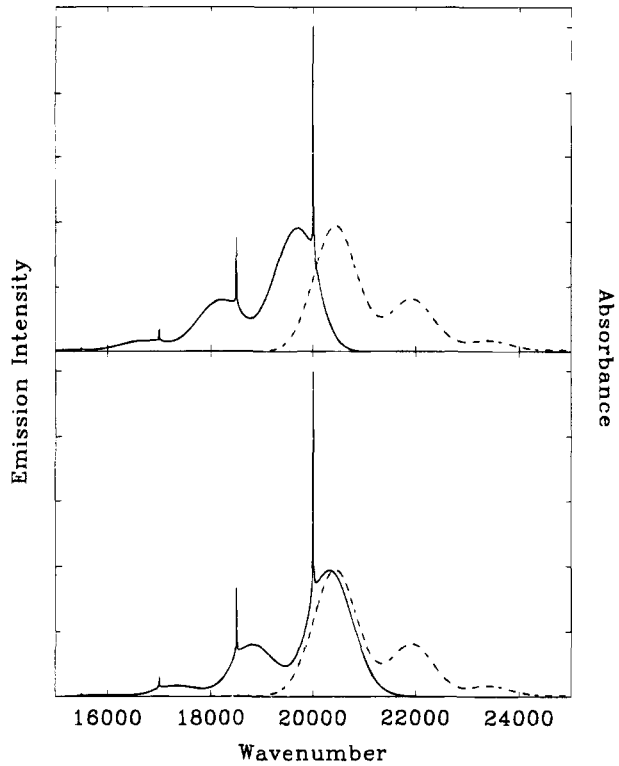

Figure 1. Absorption (dashed) and unrelaxed emission (solid) line shapes for a single-mode system with vibrational frequency 1500 cm^{-1}, dimensionless displacement $D = 0.9$, ground- and excited-state vibrational line widths of $\gamma_{ac}/2\pi c = 4$ cm^{-1} and $\gamma_{bd}/2\pi c = 10$ cm^{-1}, and vibronic line width $\gamma_{bs}/2\pi c = 10$ cm^{-1}. Top: Calculated using the Brownian oscillator model for the solvent with $\Delta_S/2\pi c = 432$ cm^{-1}, $\Lambda/2\pi c = 43.2$ cm^{-1}, and excitation at the zero−zero energy of 20 000 cm^{-1}. Bottom: The same calculation using the stochastic model with a zero-zero energy of 20 430 cm^{-1} and excitation at 20 000 cm^{-1}.

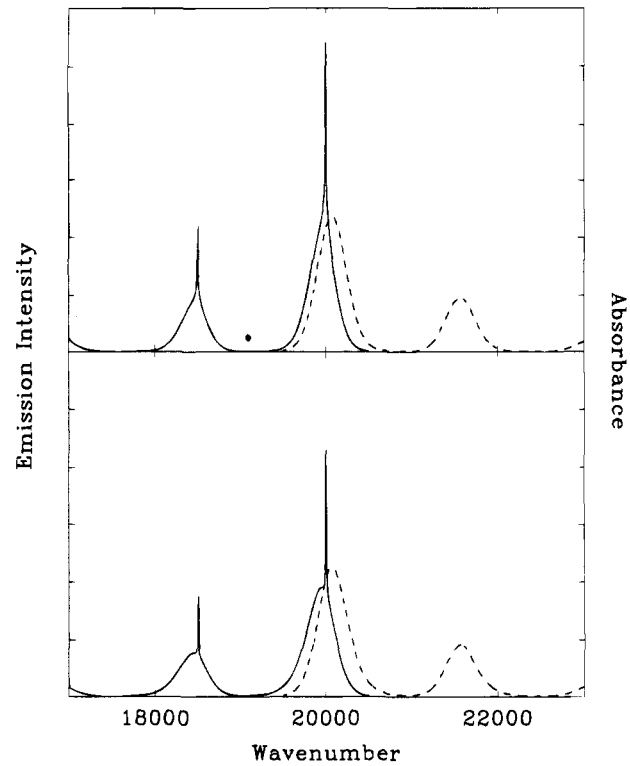

Figure 2. Absorption (dashed) and unrelaxed emission (solid) line shapes calculated using the Brownian oscillator model with a total solvent-induced line width (hwhm) of 200 cm^{-1}. Top: Intermediate time scale ($\kappa = \Lambda/\Delta_S = 0.5$). Bottom: Slow modulation ($\kappa = 0.1$). All other parameters are as in Figure 1.

maximum is blue-shifted while the emission is red-shifted relative to the zero−zero frequency of the electronic transition by approximately λ_S, while calculation with the stochastic model gives no such frequency shift.

To probe the effect of the time scale of the solvent fluctuations on the optical spectra, the emission and absorption line shapes were calculated using the Brownian oscillator model in the intermediate and slow modulation cases as shown in Figure 2. (Fast modulation, with $\kappa \geq 1$, was not explored, as it corresponds to nonphysical parameters for the Brownian oscillator; see Discussion.) A constant homogeneous line width (200 cm^{-1} half-width at half-maximum) has been employed, with the corresponding Δ_S and Λ values determined from a Padé approximant.[9] Thus for $\kappa = 0.5$ (intermediate modulation, upper panel) $\Delta_S/2\pi c = 203$ cm^{-1} and $\Lambda/2\pi c = 102$ cm^{-1}, while in the slow modulation case of $\kappa = 0.1$ (lower panel) $\Delta_S/2\pi c = 173$ cm^{-1} and $\Lambda/2\pi c = 17.3$ cm^{-1}. These solvent parameters correspond to solvent reorganization energies (λ_S) and time scales (τ_L) of 103 cm^{-1} and 52 fs for $\kappa = 0.5$, and 75 cm^{-1} and 307 fs for $\kappa = 0.1$. In the intermediate modulation calculation the absorption and fluorescence line shapes fall between Gaussian and Lorentzian in character and the frequency shift between their maxima is somewhat less than $2\lambda_S$, while with slow modulation the line shapes are Gaussian and the spectral shift between the absorption and emission maxima is approximately $2\lambda_S$. Note that while the absorption spectra for these two cases are practically indistinguishable, the emission spectra are quite different, with the distinction between the "Raman" and "fluorescence" components becoming less clear as the modulation frequency is increased.

The properties of the sharp scattering lines and the broad fluorescence bands can be further investigated by tuning the excitation frequency across the absorption band. In Figure 3, calculations of the emission line shapes using the Brownian oscillator model are shown for excitation at the zero−zero frequency and detuned by 600 and 1200 cm^{-1} to both higher and lower frequency. The solvent parameters employed are $\Delta_S/2\pi c = 432$ cm^{-1} and $\Lambda/2\pi c = 43.2$ cm^{-1}. The sharp scattering lines move as the excitation is tuned while the broad fluorescence bands stay centered at the same absolute frequency. The total integrated emission intensity is proportional to the absorption cross section at the excitation frequency (the highest-frequency sharp emission line), demonstrating that the total emission quantum yield depends only on the excited state lifetime and not on the detuning. However, the partitioning between sharp scattering and broad fluorescence does depend on detuning, with the emission becoming almost a pure Raman spectrum at a detuning of 1200 cm^{-1} to the red. Qualitatively similar behavior of the emission spectrum and the scattering to fluorescence intensity ratios as a function of detuning has been observed in a number of solution phase systems including β-carotene,[10] azulene,[11,22] and CS_2,[13] and the data have been analyzed using stochastic models for the solvent-induced broadening,[9-11,13,22] but the emission Stokes shift is missing in those treatments.

Figure 4 contrasts the relaxed (eq 15) and unrelaxed (eq 19) emission spectra. Here we have chosen an excitation frequency lying between the $0 \rightarrow 0$ and $0 \rightarrow 1$ absorption features in order to emphasize that the relaxed emission lacks not only the sharp Raman and Rayleigh bands but also the "hot" fluorescence present in the vibrationally unrelaxed spectrum.

Figures 1−4 employ parameters such that the excited-state population decay makes only a small contribution to the total electronic dephasing. Thus, for near-resonant excitation, the

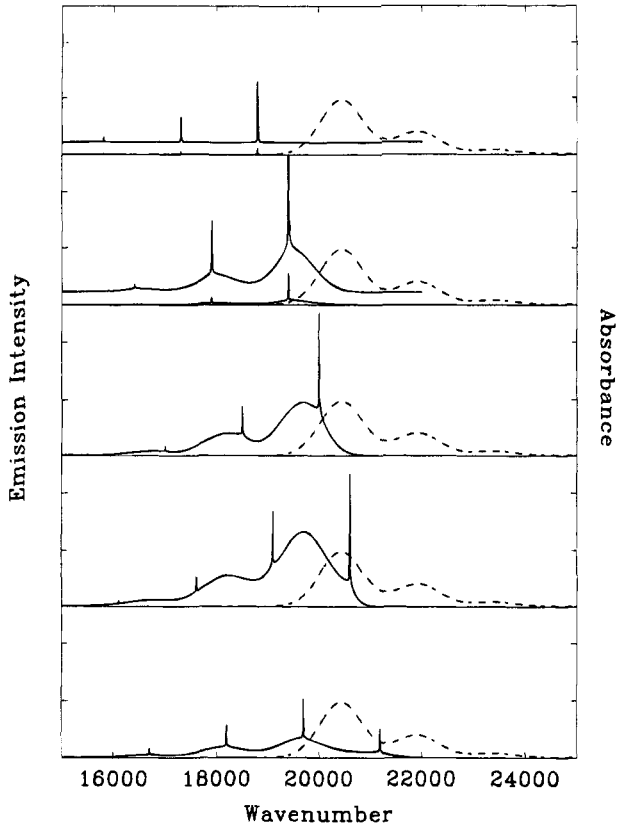

Figure 3. Absorption (dashed) and unrelaxed emission (solid) line shapes as a function of laser detuning from resonance using the Brownian oscillator model. From the top: excitation at 18 800, 19 400, 20 000, 20 600, and 21 200 cm^{-1}. Emission spectra are shown both on a common scale and expanded by a factor of 10 and offset in the top two panels. All other parameters are as given in Figure 1.

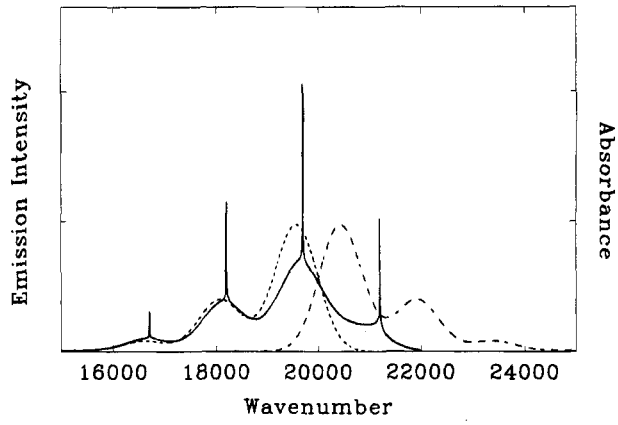

Figure 4. Absorption (long dashes), relaxed emission (short dashes), and unrelaxed emission (solid) spectra using the Brownian oscillator model at an excitation energy of 21 200 cm^{-1}. All other parameters are as in Figure 1.

sharp scattering bands constitute a small fraction of the integrated emission intensity. In Figure 5 we relax that assumption by changing $\gamma_{ba}/2\pi c$, the population decay contribution to the vibronic line width (half-width at half maximum), from 3 to 120 cm^{-1}, while holding the Brownian oscillator contribution to the width constant at 750 cm^{-1}. These parameters correspond to excited-state lifetimes of 1.83 ps to 44 fs, while the solvent relaxation time is $\tau_L = 82$ fs. As the excited-state lifetime becomes shorter, the fluorescence is strongly quenched, while the intensity of the sharp scattering is hardly affected because it depends on the total electronic dephasing, which is still dominated by the solvent dynamics. The absorption spectrum also becomes slightly broader with increasing γ_{ba} as the lifetime broadening becomes competitive with the solvent contribution. A number of experimental studies have utilized Raman to fluorescence ratios to determine or place limits on the population decay contribution to electronic dephasing rates.[11,13,19,22,37-41] In addition, closer examination shows that at the shortest lifetimes, where the lifetime is on the order of τ_L, the broad fluorescence part of the emission is considerably blue-shifted; that is, there is not enough time for the fluorescence to develop its full Stokes shift. Numerous experimental observations of time-dependent Stokes shifts have been made using fluorescence upconversion techniques,[42] and lifetime "gating" of the Stokes shift in steady-state emission experiments has also been observed.[43] Figure 5 indicates that such effects may be exposed by using a realistic Brownian oscillator model to simulate spectra of short-lived species in polar solvents.

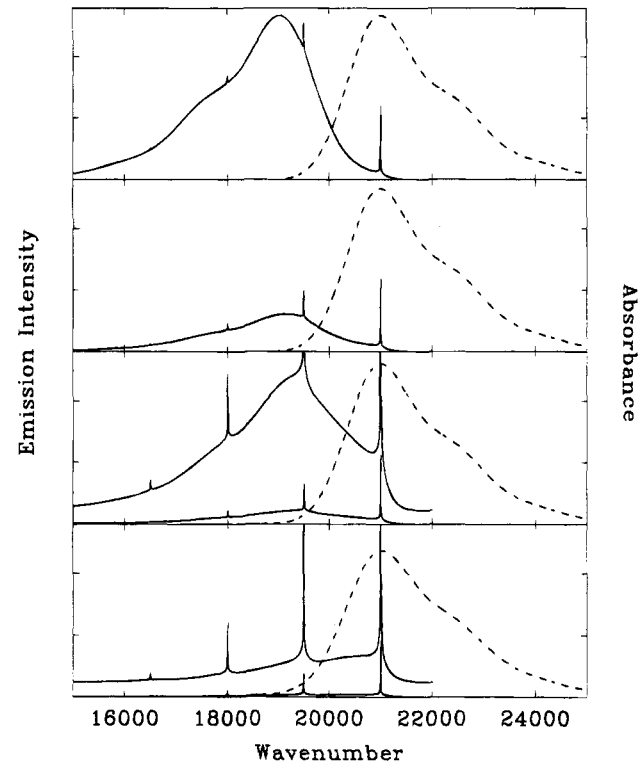

Figure 5. Absorption (dashed) and unrelaxed emission (solid) spectra as a function of excited-state lifetime using the Brownian oscillator model for the solvent with $\Delta_S/2\pi c = 648$ cm^{-1}, $\Lambda/2\pi c = 64.8$ cm^{-1}, and excitation at 21 000 cm^{-1}. From top to bottom, $\gamma_{ba}/2\pi c = 3$, 12, 30, and 120 cm^{-1}, respectively. All other parameters are as given in Figure 1. Emission spectra are shown both on a common intensity scale and expanded by a factor of 10 in the bottom two panels.

Discussion

In most applications of the Brownian oscillator model to date, it is treated as a fitting function whose parameters are varied to best reproduce experimental data. However, studies in which several different experiments on the same system are fit by a common model,[27] as well as those in which the fitting

(37) Champion, P. M.; Lange, R. *J. Chem. Phys.* **1980**, *73*, 5947.
(38) Trulson, M. O.; Dollinger, G. D.; Mathies, R. A. *J. Chem. Phys.* **1989**, *90*, 4274.
(39) Trulson, M. O.; Mathies, R. A. *J. Phys. Chem.* **1990**, *94*, 5741.
(40) Ci, X.; Pereira, M. A.; Myers, A. B. *J. Chem. Phys.* **1990**, *92*, 4708.
(41) Kulinowski, K.; Gould, I. R.; Myers, A. B. *J. Am. Chem. Soc.*, submitted for publication.
(42) Barbara, P. F.; Jarzeba, W. *Adv. Photochem.* **1990**, *15*, 1.
(43) Nagasawa, Y.; Yartsev, A. P.; Tominaga, K.; Bisht, P. B.; Johnson, A. E.; Yoshihara, K. *J. Phys. Chem.*, in press.

parameters are shown to vary in a logical way as the system is changed,[44] provide confidence that the model is physically realistic. The collective solvent and intramolecular coordinates that are important in a given system can be identified by mapping the results of molecular dynamics simulations onto this model.[45] Reference 27 contains an excellent discussion of the relationship between the Brownian oscillator model and microscopic, explicitly molecular pictures of the solvation dynamics, as well as the simpler phenomenological stochastic and Bloch equation approaches.

Since it properly incorporates the solvent contribution to the Stokes shift, the Brownian oscillator model can sensibly be applied to optical processes in charge-transfer systems as well as other electronic transitions of polar molecules in polar solvents. The underlying mechanism for solvent-induced spectral shifts in optical processes is the same one that determines the solvent reorganization process in electron transfer reactions, and the general expressions for thermally equilibrated absorption and emission (eqs 14 and 15) reduce to those commonly used to describe absorption and emission in charge-transfer transitions (eqs 24 and 25) when the static limit of the Brownian oscillator is taken. We have also shown that the Franck–Condon part of the nonadiabatic electron transfer rate, whether the solvent is taken to be in the static Gaussian limit or in general, is given by the same expression as that for thermally equilibrated fluorescence with a "zero-frequency" photon. Equation 22 may be used to calculate the nuclear contribution to the nonadiabatic electron-transfer rate with the solvent modeled as a Brownian oscillator having an arbitrary time scale.

Equation 22 does assume that the electron transfer process originates from a state that is fully relaxed along both solvent and solute coordinates. This may not provide a valid description of fast photoinduced electron transfer processes, where significant reaction may occur before intramolecular vibrational relaxation and/or solvent reorganization, and possibly even vibrational dephasing, are complete. There is considerable current interest both in modeling actual experiments in which unrelaxed electron transfer may play a role[46–49] and in exploring theoretically the phenomenology of such processes.[50] The relationship between relaxed and unrelaxed electron transfer (or other radiationless process) is conceptually similar to that between relaxed and unrelaxed light emission (eqs 15 and 19). However, while eq 22 refers to the rate of electron transfer from an equilibrated state, there does not exist a simple "rate" of reaction from a time-evolving ensemble; a different quantity, such as the time-dependent survival probability or a time-resolved pump-probe optical signal,[31,51,52] which is generally what is actually measured, has to be calculated.

The stochastic theory of line broadening describes the solvent contribution to the line shape in terms of two empirical parameters, an inverse time scale Λ and a magnitude Δ. Since there is no underlying physics connecting these parameters, they may be varied independently, and line shapes having any desired width together with a shape anywhere from purely Lorentzian to purely Gaussian can be generated. The Brownian oscillator model in the overdamped, high-temperature limit can also be cast in terms of these two parameters, as described in eqs 10–18 and their associated discussion. However, Λ and Δ_S may now no longer be varied at will, as they are related to the frequency, displacement, and friction of the underlying oscillator. In particular, the requirement that the temperature be high compared with the oscillator frequency ($\hbar\omega_B \ll k_BT$) can be shown to imply, for an overdamped oscillator, that $\hbar\Lambda < k_BT$.[31] Since $k_BT \approx 200$ cm^{-1} near room temperature and the "fast modulation" limit of Lorentzian line shapes requires $\kappa = \Lambda/\Delta > 1$, $\Delta_S/2\pi c$ cannot exceed about 100 cm^{-1}, and the corresponding solvent-induced line width of the optical transition, given by $\Delta_S^2/(2\pi c\Lambda)$ in the fast modulation limit, cannot exceed about 50 cm^{-1}. We conclude that the high-temperature, overdamped Brownian oscillator expression for $g(\tau)$ in eq 18 will never be valid in the fast modulation regime if the solvent contribution to the optical line width is significant.

A more general expression for $g(\tau)$, which still assumes an overdamped oscillator but is valid at arbitrary temperatures (e.g. arbitrary oscillator frequencies), is the following:[31]

$$g(\tau) = g_R(\tau) + ig_I(\tau) \tag{26}$$

$$g_I(\tau) = -(\lambda_S/\Lambda)[\exp(-\Lambda\tau) - 1] \tag{27}$$

$$g_R(\tau) = (\lambda_S/\Lambda)\cot(\hbar\Lambda/2k_BT)[\exp(-\Lambda\tau) + \Lambda\tau - 1] + \frac{4\lambda_S\Lambda k_BT}{\hbar}\sum_{n=1}^{\infty}\frac{\exp(-\nu_n\tau) + \nu_n\tau - 1}{\nu_n(\nu_n^2 - \Lambda^2)} \tag{28}$$

$$\nu_n = (2\pi k_BT/\hbar)n \tag{29}$$

(Equations 26–29 are derived starting from the frequency-domain spectral density for a strongly overdamped oscillator.[31] If one instead solves for the general $g(\tau)$ before taking the overdamped limit, the denominator of the summation in eq 28 becomes $\nu_n[\nu_n^2 - \Lambda^2(1 + \nu_n^2/\omega_B^2)^2]$, in agreement with the result of Champion and co-workers.[24] Numerical calculations show that inclusion of the ν_n^2/ω_B^2 correction term has a negligible effect on the band shapes plotted in Figure 6.) These expressions are straightforward enough to apply to the linear processes of absorption and thermally equilibrated emission and electron transfer, but not to calculation of the unrelaxed emission (the analog of eq 19), which involves evaluating a three-time integral. We have therefore checked the applicability of eq 18 to the conditions of our calculations by comparing the absorption band shapes calculated from the exact eqs 26–29 and the approximate eq 18, as shown in Figure 6. The parameters are the same as in Figure 1 except for the temperature. At the temperature assumed in Figure 1 ($T = 288$ K, $kT = 4.6\Lambda$) the exact calculation is nearly indistinguishable from the high-temperature approximation, but as the temperature is lowered the deviations become more substantial until, at $T = 50$ K ($kT = 0.8\Lambda$), the approximate calculation with eq 18 produces unphysical small negative lobes in the absorption spectrum. It should be noted that the high-temperature approximation works better when the total solvent-induced band width is smaller.

Since the high-temperature expressions require $\hbar\Lambda < kT$, they will be valid only when either the optical line shape is nearly Gaussian ($\kappa = \Delta_S/\Lambda \ll 1$, so Λ can be small, i.e. τ_L is long) or the solvent contribution to the line shape is small (both Δ_S and

(44) Fried, L. E.; Mukamel, S. *J. Chem. Phys.* **1992**, *96*, 116.
(45) Fried, L. E.; Bernstein, N.; Mukamel, S. *Phys. Rev. Lett.* **1992**, *68*, 1842.
(46) Tominaga, K.; Walker, G. C.; Jarzeba, W.; Barbara, P. F. *J. Phys. Chem.* **1991**, *95*, 10475.
(47) Walker, G. C.; Åkesson, E.; Johnson, A. E.; Levinger, N. E.; Barbara, P. F. *J. Phys. Chem.* **1992**, *96*, 3728.
(48) Tominaga, K.; Kliner, D. A. V.; Johnson, A. E.; Levinger, N. E.; Barbara, P. F. *J. Chem. Phys.* **1993**, *98*, 1228.
(49) Wynne, K.; Galli, C.; Hochstrasser, R. M. *J. Chem. Phys.* **1994**, *100*, 4797.
(50) Jean, J. M.; Friesner, R. A.; Fleming, G. R. *J. Chem. Phys.* **1992**, *96*, 5827.
(51) Mukamel, S. *Annu. Rev. Phys. Chem.* **1990**, *41*, 647.
(52) Johnson, A. E.; Levinger, N. E.; Jarzeba, W.; Schlief, R. E.; Kliner, D. A. V.; Barbara, P. F. *Chem. Phys.* **1993**, *176*, 555.

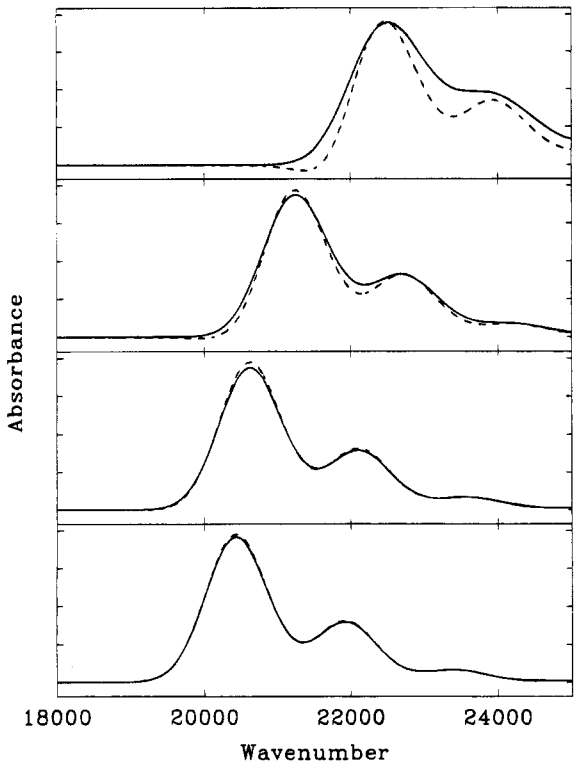

Figure 6. Comparison of absorption spectra calculated using high-temperature (eq 18, dashed curve) and arbitrary temperature (eqs 26–29, solid curve) expressions for overdamped Brownian oscillator $g(\tau)$. Parameters are the same as in Figure 1 except for the temperature. From top to bottom: $T = 50$, 100, 200, and 288 K.

Λ are small). Experimental absorption band shapes of molecules in solution provide support for this being generally true. Diffuse spectra can rarely be modeled adequately as a vibronic "stick spectrum" convolved with a broad Lorentzian;[20,53–55] a more nearly Gaussian line shape, or some intermediate shape, usually fits the data much better,[11,22,23,56] although it is often difficult to extract the purely solvent contribution to the band shape when the underlying vibronic structure of the absorption is complex. Modeling of excitation profiles and/or Raman yields using the stochastic theory also usually leads to the conclusion that the relevant solvent-induced fluctuations are in the slow to perhaps intermediate modulation regime.[8,10,11,13,21] For the solvent-induced line shape to be simultaneously hundreds of wavenumbers broad and nearly Lorentzian in shape, Λ must exceed several hundred wavenumbers, and yet the Brownian oscillator must be overdamped. Since overdamping requires the friction $\gamma \gg 2\omega_B$, and $\Lambda = \omega_B^2/\gamma$ by definition, the Brownian oscillator's frequency must satisfy the inequality $\Lambda \ll \omega_B$. Thus the frequency of the underlying solvent oscillator must exceed several hundred cm^{-1} in order to generate a broad Lorentzian line shape, and such a high frequency seems unlikely for the types of motions generally thought to contribute to most solvent reorganization and environmentally-induced dephasing processes.

We should note that there is considerable evidence from molecular dynamics simulations,[57–60] as well as some from experiments,[61,62] that at least in polar solvents, modes which are relatively high in frequency (hundreds of wavenumbers) and underdamped may contribute significantly to the solvation dynamics. However, any such high-frequency solvent modes that are strongly coupled to the electronic transition should appear in the resonance Raman spectrum in the same way that Franck–Condon active vibrations of the solute do, and they can be included in the spectral modeling on the same footing as the molecular modes. A separate model for the solvation coordinate is needed only to account for the effect of the low-frequency and/or overdamped modes that cannot be observed in the spectra directly.

It is important to stress that "slow modulation", as defined by $\Lambda/\Delta \ll 1$ and a corresponding near-Gaussian solvent contribution to the optical line shape, does not necessarily mean "static" on the resonance Raman time scale. In the limit of truly static inhomogeneous broadening ($\Lambda = 0$), there is no electronic pure dephasing, and all of the emission appears in the form of sharp lines due to Raman and Rayleigh scattering. The total emission line shapes calculated here, even in the "slow modulation" case, contain broad fluorescence bands as well as the sharp Raman and Rayleigh lines. The line width of the fluorescence part of the emission is determined by the electronic dephasing due to solvent fluctuations. Raman and Rayleigh scattering result from a coherent matter–radiation interaction in which no excited state population is generated, so these line widths are determined by the ground state vibrational lifetime. The relative intensities of the fluorescence to the Raman part of the emission decrease as the excitation is tuned away from resonance (Figure 4). This is because only near resonance can solvent fluctuations having a finite time scale act to generate a population of excited states which emit incoherently. For excitation far from resonance, the "emission time scale" is determined by the detuning to be $(\omega_{ba} - \omega_L)^{-1}$. This time scale is instantaneous as far as the solvent is concerned, and the solvent does not have enough time to dephase the optical transition. A qualitative way to explain this situation is to describe the dephasing rate as being frequency dependent; at large detunings, the dephasing vanishes. "Markovian" relaxation theories which assume frequency-independent dephasing must necessarily break down at large detunings. When both the broad fluorescence and the sharp scattering contributions to the emission can be experimentally observed, fitting the total emission line shape[21] (or, alternatively, the total scattering quantum yield)[11,13] as a function of detuning can provide detailed information regarding electronic dephasing and spectral broadening mechanisms, although complications such as preresonance contributions to the scattering must be kept in mind.

In order to avoid having to assume a specific model for vibrational energy relaxation in the excited electronic state, we have neglected it altogether in the unrelaxed emission calculations presented here, which implies that it is much slower than the assumed excited state lifetime of $\gamma_{ba}^{-1} = 0.53$ ps. This seems physically realistic, as reported vibrational energy relaxation times for molecules in liquids, while varying widely from one molecular and solvent system to another, typically exceed several picoseconds;[63–73] on the other hand, most of these values have been measured in ground electronic states,

(53) Blazej, D. C.; Peticolas, W. L. *J. Chem. Phys.* **1980**, *72*, 3134.
(54) Myers, A. B.; Mathies, R. A.; Tannor, D. J.; Heller, E. J. *J. Chem. Phys.* **1982**, *77*, 3857.
(55) Harhay, G. P.; Hudson, B. S. *J. Phys. Chem.* **1993**, *97*, 8158.
(56) Lawless, M. K.; Mathies, R. A. *J. Chem. Phys.* **1994**, *100*, 2492.
(57) Maroncelli, M. *J. Chem. Phys.* **1991**, *94*, 2084.
(58) Bader, J. S.; Chandler, D. *Chem. Phys. Lett.* **1989**, *157*, 501.
(59) Levy, R. M.; Kitchen, D. B.; Blair, J. T.; Krogh-Jespersen, K. *J. Phys. Chem.* **1990**, *94*, 4470.
(60) Schwartz, B. J.; Rossky, P. J. *J. Chem. Phys.* **1994**, *101*, 6902.
(61) Rosenthal, S. J.; Xie, X.; Du, M.; Fleming, G. R. *J. Chem. Phys.* **1991**, *95*, 4715.
(62) Deuel, H. P.; Cong, P.; Simon, J. D. Unpublished results.
(63) Paige, M. E.; Harris, C. B. *Chem. Phys.* **1990**, *149*, 37.
(64) Xu, X.; Yu, S.-C.; Lingle, R., Jr.; Zhu, H.; Hopkins, J. B. *J. Chem. Phys.* **1991**, *95*, 2445.
(65) Kliner, D. A. V.; Alfano, J. C.; Barbara, P. F. *J. Chem. Phys.* **1993**, *98*, 5375.

and excited-state vibrational relaxation may be faster. Certainly vibrational relaxation will become important for molecules with longer-lived excited electronic states and must be considered on a case by case basis in modeling experimental emission spectra.

This study demonstrates that simulations of optical absorption and emission spectra with a realistic Brownian oscillator model for the solvent coordinate can serve as a probe of electronic dephasing mechanisms in solution and can also provide a consistent description of solvent reorganization in charge transfer systems. Here we have demonstrated only calculations on a single-mode molecule, with the solvation coordinate modeled as a single effective oscillator. If one is interested only in processes that can be evaluated from a single-time integration—absorption, vibrationally relaxed emission and charge transfer, and resonance Raman when the "Raman" and "fluorescence" emission components are clearly separable[8]—it is easy to incorporate the Brownian oscillator model for solvation into realistic multimode calculations on polyatomic molecules,[23,41] and/or to use two or more solvent oscillators to model multiple time scales for spectral diffusion.[30] When the full Raman plus fluorescence emission spectrum is needed, such calculations become more involved, but the Brownian oscillator is still no more difficult computationally than the stochastic model and should be preferred because of its physical realism.

Acknowledgment. This work was supported in part by NSF grant No. CHE-9020844 to A.B.M. A.B.M. is the recipient of a Packard Fellowship in Science and Engineering, an NSF Presidential Young Investigator Award, and a Dreyfus Teacher-Scholar Award. B.L. acknowledges enlightening conversations with Professor Kevin Peters on various aspects of electron transfer.

(66) Li, M.; Owrutsky, J.; Sarisky, M.; Culver, J. P.; Yodh, A.; Hochstrasser, R. M. *J. Chem. Phys.* **1993**, *98*, 5499.
(67) Schultz, K. E.; Russell, D. J.; Harris, C. B. *J. Chem. Phys.* **1992**, *97*, 5431.
(68) Elsaesser, T.; Kaiser, W. *Annu. Rev. Phys. Chem.* **1991**, *42*, 83.
(69) Sukowski, U.; Seilmeier, A.; Elsaesser, T.; Fischer, S. F. *J. Chem. Phys.* **1990**, *93*, 4094.
(70) Sension, R. J.; Repinec, S. T.; Szarka, A. Z.; Hochstrasser, R. M. *J. Chem. Phys.* **1993**, *98*, 6291.
(71) Doorn, S. K.; Dyer, R. B.; Stoutland, P. O.; Woodruff, W. H. *J. Am. Chem. Soc.* **1993**, *115*, 6398.
(72) Phillips, D. L.; Rodier, J.-M.; Myers, A. B. *Chem. Phys.* **1993**, *175*, 1.
(73) Reid, P. J.; Wickham, S. D.; Mathies, R. A. *J. Phys. Chem.* **1992**, *96*, 5720.